2.3 kb and clone PP11 was 1.9 kb. The same fibroblast library, arrayed for PCR screening [D. J. Munroe *et al.*, *Proc. Natl. Acad. Sci. U.S.A.* **92**, 2209 (1995)], was screened with EP1R and EP1F primers; a single clone (PPc11) was characterized and found to be 2.3 kb. The brain library was screened by plaque hybridization by conventional methods [J. Sambrook, E. F. Fritsch, T. Maniatis, *Molecular Cloning: A Laboratory Manual* (Cold Spring Harbor Laboratory, Cold Spring Harbor, NY, 1989)] with the use of a 192-bp probe produced by amplification of a human lymphoblast cDNA library with the use of primers [5′-TCACTGAGGACACACCCTCG-3′ (nt 738 to 757) and 5′-GGTAGATATAGGTGAAGAGG-3′ (nt 929 to 910)] complementary to T03796. Three clones were obtained from the brain library: PS2-41 (2.3 kb), PS2-6 (1.9 kb), and PS2-10 (1.7 kb).

14. Three fibroblast cDNA clones (PPc11, PP15A, and PP11) were sequenced as follows. The cDNA fragments in pBK-CMV (Stratagene) were excised from agarose gels, purified with a Gene-Clean kit (Bio-101), and fragmented by flow extrusion in high-performance liquid chromatography (P. Oefner, personal communication) to a size range of 0.5 to 1 kb. These fragments were cloned directly into M13mp18 (Novagen) cut by Sma I and phosphatased with the use of the manufacturer's protocols. The resulting plaques were picked into PCR buffer and amplified with primers homologous to the vector. The PCR products were purified on a G-50 spin column and sequenced with Applied Biosystems forward and reverse dye-primer sequencing kits. Samples were run on an Applied Biosystems 373 A sequencer. The data were assembled with DNAStar, with the translated coding region shown in Fig. 3. Three brain cDNA clones (PS2-41, PS2-6, and PS2-10) were sequenced manually with Sequenase from U. S. Biochemical. The DNA sequence has been deposited in GenBank (accession number L43964). The nucleotide numbering used here is based on the ATG codon being at nt 368 to 370.
15. A Northern blot (Clontech) containing 2 μg of human polyadenylated mRNA derived from heart, brain, placenta, lung, liver, skeletal muscle, and pancreas was hybridized with the 2.3-kb F-T03796 cDNA clone as a probe. Hybridization was in 0.75 M NaCl, 0.05 M NaH_2PO_4, 5 mM Na_2EDTA, ×10 Denhardt's solution, 100 μg/ml salmon sperm DNA, 50% formamide, and 2% SDS at 42°C for 18 hours. Filters were washed with ×0.1 saline sodium citrate and 0.1% SDS at 65°C. The two transcripts observed are possibly the result of alternative polyadenylation because two putative polyadenylation signals were identified in the 3′ untranslated region, starting at nucleotides 1834 and 2309 (*14*). The message sizes for STM2 from Northern blot analysis (2.4 and 2.8 kb) were larger than the 2.3-kb size predicted from the full-length DNA sequence and the 1.8-kb size predicted by the second polyadenylation site observed in that sequence. This discrepancy is possibly due to the anomalous migration of size markers that has been previously observed with this type of Northern blot.
16. Reverse transcription (RT)–PCR products synthesized from RNA (Becton Dickinson Mini RiboSep) prepared from affected VG subjects and controls were amplified with a variety of primers and the PCR products cycle-sequenced with the Promega fmol DNA Sequencing System. In other experiments, RT-PCR products were gel-purified, re-amplified with the same primers, and sequenced with a U.S. Biochemicals Sequenase PCR Product sequencing kit. In addition to the N141I mutation, three sequence variants were identified at nucleotides 436 (C/T, HB subject), 496, (C/T, HD and W subjects), and 628 (C/T, HD and W subjects). These variants did not change the amino acid encoded at these sites (alanine, asparagine, and histidine, respectively).
17. An upper confidence bound on the mutation gene frequency, p, when no mutations are found, can be found with the equation $(1 - p)^N = \alpha$, where N is the number of chromosomes tested and α is the desired significance level. A 95% upper confidence limit for the N141I mutation frequency is 0.0077, based on no mutations observed in 195 independent controls.
18. Lod scores for the age-dependent penetrance model were computed as described (*4*). For the general sporadic model, the program LIPED was modified to correct for phenocopies (*7*) caused by possible sporadic AD by taking actual age of onset into account [P. Margaritte *et al.*, *Am. J. Hum. Genet.* **50**, 1231 (1992)] and with the assumption of a mean sporadic onset age of 110 years and a standard deviation of 20 years. We obtained these values for the sporadic rate by maximizing the likelihood of the data in the presence of linkage to D1S479 (*4*). For the covariate sporadic model, an additional modification to LIPED allowed use of the APOE genotype as a covariate, so that the APOE ε4/ε4 genotype was assumed to have a lower sporadic mean onset than the general population sporadic onset. An AD allele frequency of 0.001, a N141I allele frequency of 0.0077, and a mean sporadic onset age for APOE ε4/ε4 ranging in 5-year increments from 70 to 100 were used.
19. F. C. Clerget-Darpoux, C. Bonaiti-Pellie, J. Hochez, *Biometrics* **42**, 393 (1986).
20. S. M. L'Hernault and P. M. Arduengo, *J. Cell Biol.* **119**, 55 (1992).
21. D. Scheuner, *et al.*, *Soc. Neurosci. Abstr.*, in press; X.-H. Song *et al.*, *ibid.*, in press.
22. Supported by grants from the National Institute on Aging for the Alzheimer's Diseases Research Center at the University of Washington (AG0513C) and grants RO1-AG11762 (G.D.S.) RO1-AG11899 (W.W.), and RO1-NS30428 (R.E.T.), Veterans Affairs Research Funds, and National Research Service Award postdoctoral fellowship F32 AG05635 (E.L.-L.), the American Health Assistance Foundation (G.D.S. and R.E.T.), the French Foundation (R.E.T.), and an American Physicians Fellowship (E.L.-L.). W.W. is a Becton-Dickinson Fellow and R.E.T. is a Pew scholar in Biomedical Sciences. We thank D. Nochlin, M. Sumi, M. Ball, and G. Glenner for neuropathologic characterization of many of the families, A. Lahad for statistical consultations, E. Loomis, L.-J. Anderson, E. Jeffrey, B. Paeper, T. Britschgi, L. Gordon, and R. Alish for technical help, H. Lipe and T. Lampe for obtaining blood samples and medical records, M. Boehnke and A. Motulsky for reading the manuscript before publication, J. Mulligan for much help and advice, M. Brunkow for helpful discussion, and R. Jones for help in the sequence analysis. Informed consent was obtained from each subject or next of kin with approval of the University of Washington Human Subjects Review Committee. We also thank the many family members who generously cooperated in this study, the American Historical Society of Germans from Russia, and T. Kloberdanz, G. Miner, and R. Cook-Deegan.

17 July 1995; accepted 24 July 1995

Ionic Mechanisms of Neuronal Excitation by Inhibitory $GABA_A$ Receptors

Kevin J. Staley,* Brandi L. Soldo,† William R. Proctor

Gamma-aminobutyric acid A ($GABA_A$) receptors are the principal mediators of synaptic inhibition, and yet when intensely activated, dendritic $GABA_A$ receptors excite rather than inhibit neurons. The membrane depolarization mediated by $GABA_A$ receptors is a result of the differential, activity-dependent collapse of the opposing concentration gradients of chloride and bicarbonate, the anions that permeate the $GABA_A$ ionophore. Because this depolarization diminishes the voltage-dependent block of the *N*-methyl-D-aspartate (NMDA) receptor by magnesium, the activity-dependent depolarization mediated by GABA is sufficient to account for frequency modulation of synaptic NMDA receptor activation. Anionic gradient shifts may represent a mechanism whereby the rate and coherence of synaptic activity determine whether dendritic $GABA_A$ receptor activation is excitatory or inhibitory.

Transient decreases in inhibition are necessary for the induction of plasticity at Hebbian synapses (*1*). High-frequency stimulation, which mimics the in vivo firing frequencies of the interneurons that release GABA (*2*), is the most robust method of increasing synaptic strength (*1*). $GABA_A$ receptor activation, which is normally inhibitory (*3*), becomes excitatory at these high frequencies because the postsynaptic membrane is depolarized rather than hyperpolarized (*4*–*6*). The mechanism of this depolarization is unknown but should involve the flux of chloride (Cl^-) and bicarbonate (HCO_3^-) because the $GABA_A$ ionophore is selectively permeable to these anions (*7*, *8*). Although some classes of neurons maintain a resting Cl^- reversal potential (E_{Cl}) that is more positive than the resting membrane potential (RMP) (*3*, *9*, *10*), in neurons such as pyramidal cells that maintain E_{Cl} negative to the RMP, regional (*11*) and activity-dependent (*12*) differences in the cytoplasmic Cl^- concentration ($[Cl^-]_i$) are not sufficient to explain the activity-dependent $GABA_A$ receptor–mediated depolarization (*13*, *14*). The HCO_3^- reversal potential (E_{HCO_3}) is much more positive than the RMP (*15*), but efforts to define a role for HCO_3^- in the GABA-mediated depolarization have been inconclusive (*16*), as it has not been possible to reconcile a depolarizing HCO_3^- efflux with the salient characteristics of the GABA-mediated depolarization: activity dependence, slow kinetics, and dendritic localization (*4*–*6*).

K. J. Staley, Departments of Neurology and Pediatrics B182, University of Colorado Health Sciences Center, 4200 East 9th Avenue, Denver, CO 80262, USA.
B. L. Soldo and W. R. Proctor, Department of Pharmacology, University of Colorado Health Sciences Center, and Denver VA Medical Center, Denver, CO 80262, USA.

*To whom correspondence should be addressed.
†Present address: Department of Physiology, University of Michigan Medical School, Ann Arbor, MI 48109, USA.

We propose that GABA-mediated excitation is due to an activity-dependent shift of the $GABA_A$ reversal potential (E_{GABA}) toward E_{HCO_3}. The resting E_{GABA} is primarily determined by E_{Cl} because the permeability of Cl^- is five times that of HCO_3^- (*7*). However, intense $GABA_A$ receptor activation produces millimolar shifts in the concentrations of permeant anions, as demonstrated by the HCO_3^--dependent extracellular alkalization of up to 0.2 pH units measured under these conditions (*17*). Efflux of HCO_3^- and influx of Cl^- through the $GABA_A$ ionophore would lead to an accumulation of Cl^- inside the neuron (*12*) and an accumulation of HCO_3^- outside (Fig. 1A) (*17*). Although the shift in the Cl^- gradient is eventually corrected (*12, 14*), the HCO_3^- flux is more rapidly compensated by intracellular and extracellular pH buffers acting in conjunction with the diffusion of CO_2 back across the membrane, where intraneuronal carbonic anhydrase (*18*) catalyzes the regeneration of HCO_3^-. Thus, with intense $GABA_A$ receptor activation, the electrochemical gradient for Cl^- collapses more significantly than does the HCO_3^- gradient, producing a shift in E_{GABA} toward E_{HCO_3} that is sufficient to explain the depolarizing response (Fig. 1B). This model predicts that the shift in E_{GABA} will be slow and will be increased by any condition that increases the open time of the $GABA_A$ channel (*19*). Furthermore, the shift in E_{GABA} will be larger in structures such as dendrites (*4, 5*) that have a low ratio of volume-to-receptor density because $[Cl^-]_i$ will be more easily affected by $GABA_A$ receptor–mediated currents (*20*) and CO_2 can more rapidly diffuse from the extracellular to the intracellular space to reform intracellular HCO_3^-.

We tested this model in vitro with adult rat hippocampal slices. Selective activation of $GABA_A$ receptors on the distal dendrites of CA1 pyramidal neurons (*21*) evoked by a single stimulus in the stratum moleculare always produced a hyperpolarizing membrane potential response ($n = 64$). However, when the stimulus frequency was increased to resemble the in vivo burst firing rate of hippocampal inhibitory interneurons (a 200-Hz, 200-ms train) (*2*), a larger hyperpolarizing response was followed by a slow depolarizing potential that was as much as 20 mV positive to the RMP ($n = 16$) (Fig. 2A) (*4, 5*). The activity dependence of the GABAergic depolarization was synapse-specific: Additional stimuli applied to other groups of synapses did not elicit further depolarization as effectively as additional stimuli applied to the originally stimulated synapses ($n = 4$) (Fig. 2B).

When concentrations of CO_2 and HCO_3^- in the brain slice were minimized by incubation in artificial cerebrospinal fluid (ACSF) buffered with Hepes and 100% O_2, the RMP changed on average by less than 1 mV, but reproducible depolarizing $GABA_A$ responses could not be obtained to single (*14*) or tetanic ($n = 4$) stimuli. This result was not due to presynaptic effects of the buffer change (*16*) because pressure application of the selective $GABA_A$ receptor

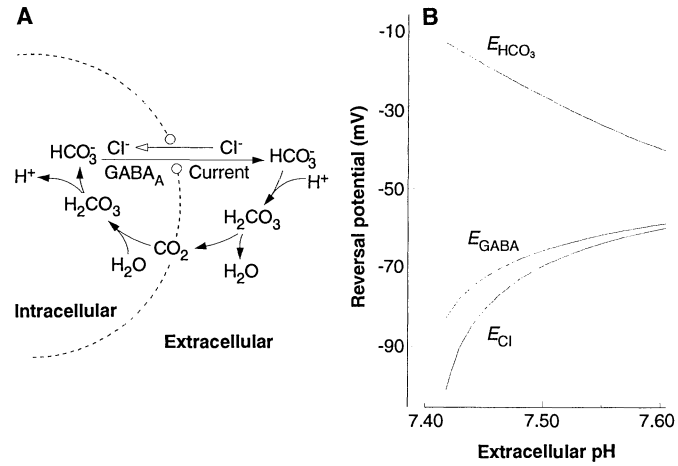

Fig. 1. Mechanisms of GABA-mediated membrane depolarization. (**A**) Differential anionic concentration shifts during intense $GABA_A$ receptor activation. The membrane potential is positive to E_{Cl} (*12, 14*), so that the Cl^- flux is inward and $[Cl^-]_i$ increases, but the membrane potential is negative to E_{HCO_3} (*7*), so that $[HCO_3^-]_i$ decreases due to the efflux of HCO_3^-. The decrease in $[HCO_3^-]_i$ drives the diffusion of CO_2 across the dendritic membrane, allowing continual regeneration of intracellular HCO_3^- by carbonic anhydrase at a rate that exceeds the removal of intracellular Cl^- (*12, 14*). (**B**) Estimation of the depolarizing shift in E_{GABA} resulting from the ionic shifts associated with the extracellular pH increase of 0.2 measured during intense $GABA_A$ receptor activation (*17*). A shift in E_{GABA} from −82 to −58 mV, an increase in the extracellular concentration of HCO_3^- ($[HCO_3^-]_e$) of 2 mM, and an increase in $[Cl^-]_i$ of 10 mM is predicted on the basis of the following assumptions: (i) the pH shift is due to HCO_3^- efflux through the $GABA_A$ ionophore, where $pH = pK + \log([HCO_3^-]/[CO_2])$; (ii) a ratio of extracellular volume to active dendritic volume of 5:1; (iii) the $[Cl^-]_i$ increase from a resting value of 3 mM is scaled to the $[HCO_3^-]_e$ increase on the basis of three factors: the intracellular-to-extracellular volume ratio, the driving force ratio ($E_{GABA} - E_{Cl}$ versus $E_{GABA} - E_{HCO_3}$), and a HCO_3^--to-Cl^- permeability ratio of 0.2 (*7*); (iv) $E_{GABA} = (RT/F)\ln[([Cl^-]_e + 0.2[HCO_3^-]_e)/([Cl^-]_i + 0.2[HCO_3^-]_i)]$, where R is the gas constant, T is temperature, and F is the Faraday. (*7, 32*); (v) regeneration of intracellular HCO_3^- diminishes the change in $[HCO_3^-]_i$ by a factor of 2 [see (A) and Fig. 3C]; and (vi) the $[CO_2]_e$ decreases as a result of CO_2 diffusion into the intracellular space [see (A)], consistent with effects of carbonic anhydrase inhibitors on the extracellular pH shift (*17*).

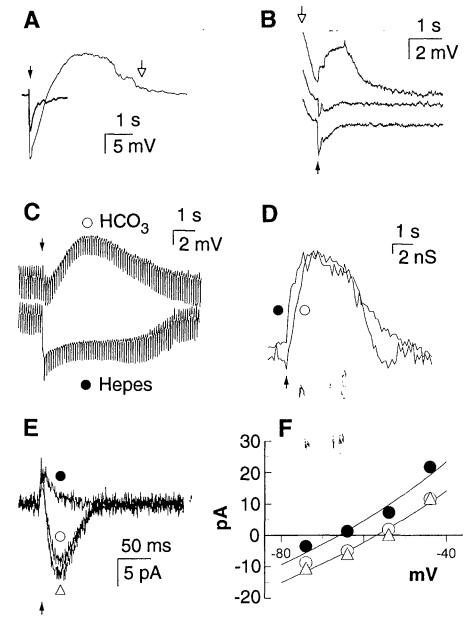

Fig. 2. Activity and HCO_3^- dependence of the late depolarizing response to $GABA_A$ receptor activation. (**A**) Selective activation of $GABA_A$ receptors by single distal orthodromic stimuli (indicated here and in subsequent figures by a solid arrow) produces hyperpolarizing $GABA_A$ receptor–mediated postsynaptic potentials (heavy line), but a train of 40 stimuli at 200 Hz produces an additional late depolarizing potential in a CA1 pyramidal cell (RMP of −72 mV). (**B**) In another neuron, a second stimulus train applied during the decay of the depolarization [timing indicated by open arrow in (A)] produced a depolarization when the second stimulus was applied to the same dendritic location (top), a small hyperpolarization and depolarization when applied to another distal dendritic area (middle), and only hyperpolarization when applied in the proximal molecular layer (bottom). (**C**) Muscimol applied to the distal dendrites of CA1 pyramidal cells produces a depolarizing response in HCO_3^- buffer (○, RMP of −67 mV) and a hyperpolarizing response in Hepes buffer (●, RMP of −69 mV). Conductance was monitored by the membrane potential response to 20 ms, −120-pA pulses delivered at 10 Hz. (**D**) The calculated increase in input conductance induced by $GABA_A$ receptor activation [panel (C)] was the same in Hepes (●) and HCO_3^- (○). (**E**) In HCO_3^- buffer, the late inward current produced by GABA application to the distal dendrites of a neocortical pyramidal cell voltage-clamped at −64 mV is not seen when the buffer is switched from HCO_3^- (○, and wash, △) to Hepes (●). (**F**) The current-voltage plot demonstrates that changing to Hepes buffer (●) produces a −10-mV shift in the reversal potential of the GABA response compared with HCO_3^- buffer (○, and wash, △).

agonist muscimol in the stratum moleculare produced only hyperpolarizing responses in Hepes (n = 10) despite increases in the input conductance that were equal to or greater than the increases produced in ACSF buffered with HCO_3^- and CO_2 (n = 70) (Fig. 2, C and D). In voltage-clamped neocortical pyramidal cells, the reversal potential of the late response to dendritic applications of GABA shifted by an average of −16 mV when the ACSF buffer was switched from HCO_3^- and CO_2 to Hepes (n = 2) (Fig. 2, E and F) (*22*). The depolarizing response to dendritic muscimol application in CA1 pyramidal cells in HCO_3^--CO_2–buffered ACSF was increased when the Cl^- in the ACSF was replaced with isethionate (n = 4), but the response was not blocked by Na^+ channel antagonists including tetrodotoxin (n = 9) and QX314 (n = 19), inhibition of cation-Cl^- cotransport with 50 μM bumetanide (n = 2), inhibition of Cl^--HCO_3^- exchange with 500 μM 4-acetamido-4′-isothiocyanatostilbene-2,2′-disulfonic acid (SITS) (n = 7), substitution of extracellular Ca^{2+} with Mg^{2+} (n = 2), nor inhibition of the sodium-potassium adenosine triphosphatase with 10 μM ouabain (n = 3).

The proposed anionic gradient shift model predicts that the depolarizing effect of intense $GABA_A$ receptor activation will be diminished by decreasing the rate of intracellular HCO_3^- regeneration, either by reducing the rate of hydration and dehydration of CO_2, or by increasing $[H^+]_i$, which decreases $[HCO_3^-]_i$ (Fig. 1A). Amiloride, which increases neuronal H^+ by inhibiting neuronal Na^+-H^+ exchange (*23*), blocked the depolarizing response to $GABA_A$ receptor activation (n = 4) (Fig. 3A). Voltage clamp experiments demonstrated that amiloride shifted the reversal potential of the $GABA_A$ response by an average of −33 mV with no significant effect on the $GABA_A$ conductance (n = 5) (Fig. 3B), consistent with a decrease in $[HCO_3]_i$.

Blocking HCO_3^- regeneration by inhib-

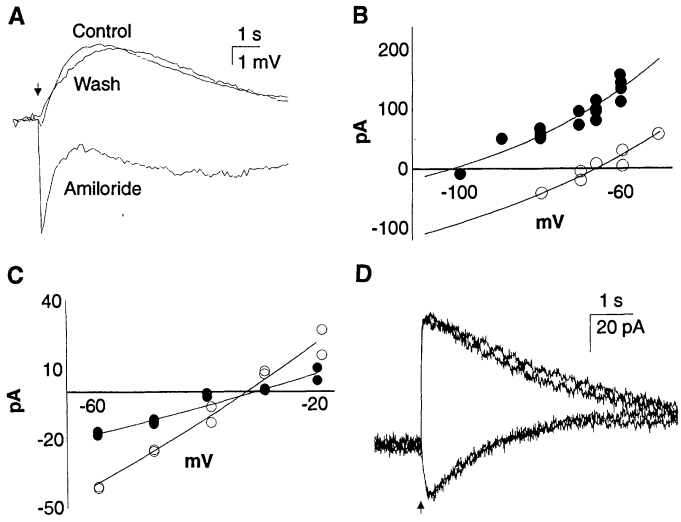

Fig. 3. Role of HCO_3^- efflux and regeneration in the depolarizing $GABA_A$ response. (**A**) The $GABA_A$ receptor–mediated depolarizing response to muscimol application to the distal dendrites of a CA1 pyramidal neuron in HCO_3^- buffer is reversibly blocked by increasing $[H^+]_i$ with 1 mM amiloride, which inhibits Na^+-H^+ exchange. (**B**) In a voltage-clamped CA1 pyramidal cell in HCO_3^- buffer, the reversal potential of the $GABA_A$ receptor–mediated current induced by muscimol application (○) is shifted −30 mV by 1 mM amiloride (●). (**C**) In a similar experiment performed in HCO_3^--buffered ACSF in which isethionate replaced all but 4 mM Cl^- (○), 10 μM acetazolamide (●) decreased the conductance induced by $GABA_A$ receptor activation but did not affect the reversal potential. (**D**) In Hepes buffer, the currents induced by muscimol application to the distal dendrites of a CA1 pyramidal cell at −70 mV (upper records) and −80 mV (lower records) (*33*) are superimposed on the currents recorded in 10 μM acetazolamide plus 1 mM amiloride, indicating that these agents have no direct effect on the $GABA_A$ receptor–mediated conductance.

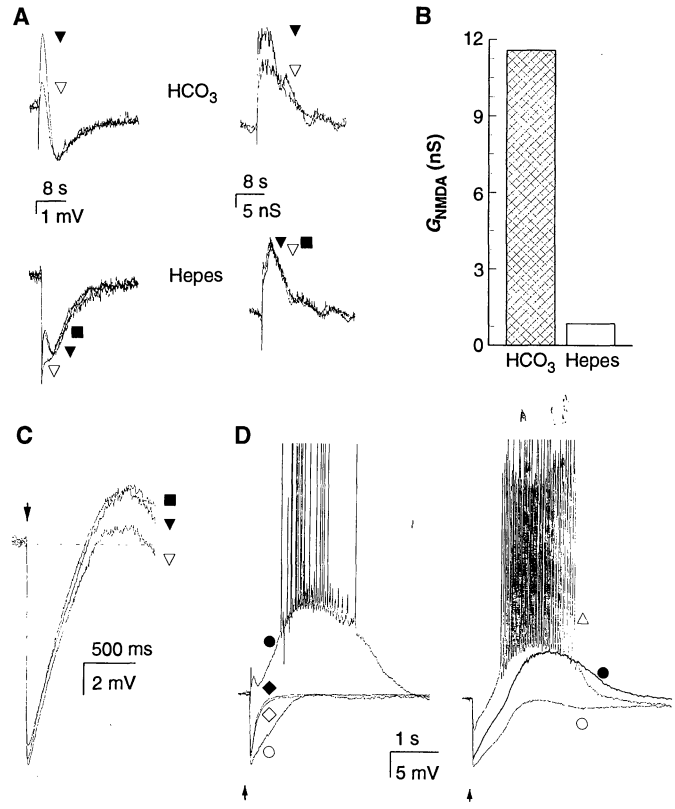

Fig. 4. The depolarizing $GABA_A$ response regulates the amplitude of the NMDA conductance when both receptors are activated. (**A**) Recordings of membrane potential (left panels) and input conductance (right panels) responses to the application of 250 μM muscimol + 250 μM NMDA to the distal dendrites of a single CA1 pyramidal cell (RMP of −69 mV) in ACSF buffered with HCO_3^- (top panels) and Hepes (bottom panels). Control ACSFs contained 20 μM DNQX and 100 μM CGP-35348 (▼). Bath application of the NMDA receptor antagonist DL-2-amino-5-phosphonovaleric acid (APV, 50 μM, ▽) has a much larger effect on membrane potential and input conductance responses in ACSF buffered with HCO_3^- than with Hepes. Responses on return to control Hepes ACSF (wash) are also shown (■). Input conductance was monitored by current pulses as in Fig. 2C. (**B**) NMDA receptor responses in (A) were obtained by subtracting the response in APV from the response in control solution. The time-averaged NMDA receptor–mediated conductance (G_{NMDA}) is over 12 times as large in HCO_3^- compared with Hepes-buffered ACSF. (**C**) NMDA receptor–mediated component of the membrane depolarization induced by high-frequency synaptic activation of NMDA and $GABA_A$ receptors. Same conditions as Fig. 2A, but without kynurenic acid: control (▼), 40 μM APV (▽), and wash (■). Peak depolarization in APV (42% of control, n = 5) was similar to the APV effect (35% of control depolarization, n = 4) when NMDA and $GABA_A$ receptors were nonsynaptically activated in HCO_3^- media [see (A)]. (**D**) $GABA_A$ receptor–mediated depolarization is sufficient to modulate the voltage-dependent Mg^{2+} block of synaptic NMDA receptor activation. Conditions as in (C). At left, single stimuli evoke an inhibitory postsynaptic potential (◇) that is not affected by acetazolamide (◆). In the left and right panels, high-frequency stimuli evoke robust depolarizations (●). GABA-mediated depolarization is necessary for this response, because in 10 μM acetazolamide, tetanic stimuli produce only hyperpolarizations (○). When the Mg^{2+} block of the NMDA receptor was diminished by removing Mg^{2+} from the ACSF, tetanic stimuli produced NMDA receptor–mediated depolarizations despite the presence of 10 μM acetazolamide (right panel, △), indicating that the NMDA receptor–mediated component of the response is determined by the degree to which the voltage-dependent Mg^{2+} block is relieved by the activity-dependent $GABA_A$ receptor–mediated depolarization.

iting carbonic anhydrase with acetazolamide led to the activity-dependent collapse of the HCO_3^- gradient. Thus, $GABA_A$ receptor–mediated HCO_3^- currents decayed more rapidly, so that the apparent GABA conductance decreased by a factor of 2.5, and the reversal potential shifted toward E_{Cl} (n = 4) (*24*). Acetazolamide produced a similar decrease in apparent conductance when the experiment was repeated in low-[Cl^-] ACSF, although in the absence of a Cl^- flux there was no shift in the reversal potential (n = 3) (Fig. 3C), indicating that acetazolamide does not affect the resting HCO_3^- gradient. Single $GABA_A$ postsynaptic currents evoked in HCO_3^--buffered ACSF did not transfer enough charge to affect the anionic gradients and thus were unaffected by acetazolamide (n = 6). Neither amiloride nor acetazolamide altered Cl^- homeostasis because they did not affect large, muscimol-evoked currents in Hepes-buffered ACSF (n = 5) (Fig. 3D). These results, together with the data from earlier studies (*16*), support the model illustrated in Fig. 1 and demonstrate that both GABAergic HCO_3^- permeability and differential maintenance of the [HCO_3^-] versus [Cl^-] gradients are necessary for activity-dependent, $GABA_A$ receptor–mediated depolarization.

The depolarization of distal dendrites as a result of HCO_3^- efflux during prolonged $GABA_A$ receptor activation will be underestimated by recordings from the soma because of shunting by $GABA_A$ receptor–mediated conductances (*10*) in larger, more proximal dendrites, where the ionic gradients are more stable (*20*). One consequence of this distal-to-proximal membrane potential gradient is that the voltage-dependent Mg^{2+} block of the *N*-methyl-D-aspartate (NMDA) receptor (*25*) will be preferentially lessened in those dendrites with the most intense $GABA_A$ receptor activation. This effect is demonstrated in Fig. 4, A and B: The NMDA receptor–mediated conductance is increased on average by a factor of 10 by GABA-mediated dendritic depolarization (n = 4), an increase that is many times larger than, but synergistic with, the increased NMDA conductance produced by the alkalization of the extracellular pH (*26*) due to HCO_3^- efflux (*17*).

These results suggest that one function of the GABA-mediated depolarization may be to provide activity-dependent modulation of the Mg^{2+} block of the NMDA receptor. When $GABA_A$ and NMDA receptors are selectively activated by high-frequency synaptic stimulation in HCO_3^- buffer, a large component of the resulting membrane depolarization is due to NMDA receptor activation (Fig. 4C), which is modulated by the interaction between the GABA-mediated depolarization and the voltage-dependent Mg^{2+} block of the NMDA receptor (Fig. 4D). These results, together with the finding that agents that increase GABA release enhance the induction of synaptic alterations by high-frequency synaptic activation (*27*), suggest that the frequency modulation of $GABA_A$ receptor function produced by physiological rates of GABA release (*2*) may play a role in regulating NMDA-dependent mechanisms of synaptic plasticity (*1*). This role can be evaluated with agents such as acetazolamide that block GABA-mediated excitation without affecting GABA-mediated inhibition (Figs. 3 and 4D). Acetazolamide also reduces network excitability in the human brain (*28*), suggesting that the frequency modulation of GABA receptor function may contribute to the recently described synchronization of neural networks by inhibitory interneurons (*29*).

Note added in proof: The recent demonstration of increased synaptic release and decreased reuptake of GABA in human epileptic hippocampus (*31*) support the possibility that activity-dependent GABA-mediated excitation is similarly increased (*19*), which may contribute to epileptogenesis.

REFERENCES AND NOTES

1. T. V. P. Bliss and G. L. Collingridge, *Nature* **361**, 31 (1993).
2. G. Buzsáki, Z. Horvath, R. Urioste, J. Hetke, K. Wise, *Science* **256**, 1025 (1992).
3. U. Misgeld *et al.*, *ibid.* **232**, 1413 (1986).
4. B. E. Alger and R. A. Nicoll, *J. Physiol. (London)* **328**, 125 (1982).
5. R. K. S. Wong and D. J. Watkins, *J. Neurophysiol.* **48**, 938 (1982); Y. Ben-Ari *et al.*, *J. Physiol. (London)* **416**, 303 (1989); H. B. Michelson and R. K. S. Wong, *Science* **253**, 1420 (1991); N. A. Lambert *et al.*, *J. Neurophysiol.* **66**, 1538 (1991); X. Xie and T. G. Smart, *J. Physiol. (London)* **460**, 503 (1993); C. H. Davies and G. L. Collingridge, *ibid.* **472**, 245 (1993); E. H. Buhl *et al.*, *Nature* **368**, 823 (1994).
6. R. H. Thalmann, *Neurosci. Lett.* **21**, 319 (1988).
7. J. Bormann, O. P. Hamill, B. Sakmann, *J. Physiol. (London)* **385**, 243 (1987).
8. K. Kaila and J. Voipio, *Nature* **330**, 163 (187); F. J. Alvarez-Leefmans, in *Chloride Channels and Carriers in Nerve, Muscle, and Glial Cells*, F. J. Alvarez-Leefmans and J. M. Russel, Eds. (Plenum, New York, 1990); K. Kaila *et al.*, *J. Physiol. (London)* **464**, 273 (1993).
9. R. A. Nicoll, *J. Physiol. (London)* **283**, 121 (1978); F. J. Alvarez-Leefmans *et al.*, *ibid.* **406**, 225 (1988).
10. K. J. Staley and I. Mody, *J. Neurophysiol.* **68**, 197 (1992).
11. W. Müller *et al.*, *Brain Res.* **484**, 184 (1989).
12. J. R. Hugenard and B. E. Alger, *J. Neurophysiol.* **56**, 1 (1986); S. M. Thompson and B. H. Gahwiler, *ibid.* **61**, 501 (1989).
13. Selective $GABA_A$ receptor activation in neurons with a resting E_{Cl} negative to the RMP will lead to neuronal Cl^- accumulation due to Cl^- influx through the $GABA_A$ ionophore. This Cl^- influx drives E_{Cl} toward the RMP, but it cannot drive E_{Cl} positive to the RMP. Neurons, including hippocampal pyramidal cells, that express the ClC-2 inwardly rectifying Cl^- conductance cannot accumulate a resting regional Cl^- concentration sufficient to cause a depolarizing $GABA_A$ receptor–mediated Cl^- flux (*14*).
14. K. J. Staley, *J. Neurophysiol.* **72**, 273 (1994).
15. The reversal potential of HCO_3^- (E_{HCO_3}) is determined by the transmembrane pH gradient, because HCO_3^- is in equilibrium with H^+ and with CO_2, and CO_2 is freely diffusible across the neuronal membrane (Fig. 1A). At physiologic extracellular and intracellular pH values of 7.4 and 7.2, respectively, and equal $[CO_2]_e$ and $[CO_2]_i$, the Henderson-Hasselbalch equation indicates that $[HCO_3^-]_i$ will be 16 mM $[HCO_3^-]_e$ will be 26 mM, and therefore the Nernst equation predicts a E_{HCO_3} of −12 mV. Thus, $GABA_A$ receptor–mediated HCO_3^- flux will be outward and depolarizing at membrane potentials near the RMP.
16. L. M. Grover, N. A. Lambert, P. A. Schwartzkroin, T. J. Teyler, *J. Neurophysiol.* **69**, 1541 (1993).
17. J. C. T. Chen and M. Chesler, *ibid.* **67**, 29 (1992); W. Jarolimek *et al.*, *Brain Res.* **505**, 225 (1989); K. Kaila *et al.*, *Neuroreport* **3**, 105 (1992).
18. M. Pasternack, J. Voipio, K. Kaila, *Acta Physiol. Scand.* **148**, 229 (1993).
19. The depolarizing response has been augmented by a variety of manipulations, all of which increase the open time of the $GABA_A$ ionophore: increasing the amount of GABA released by inducing bursting in interneurons [M. Avoli and P. Perreault, *Brain Res.* **400**, 191 (1987); W. Müller and U. Misgeld, *J. Neurophysiol.* **65**, 141 (1991)] or by high-frequency stimulation (*5*); inhibiting GABA reuptake (*4*); application of exogenous agonist (*4, 5*); and increasing the $GABA_A$ ionophore open time postsynaptically with barbiturates (*4, 6*).
20. N. Qian and T. Sejnowski, *Proc. Natl. Acad. Sci. U.S.A.* **87**, 8145 (1990).
21. Whole-cell recordings were performed in brain slices prepared from adult rats by standard methods as described [K. J. Staley, T. S. Otis, I. Mody, *J. Neurophysiol.* **67**, 1346 (1992)]. HCO_3^--buffered ACSF was saturated with 95% O_2 and 5% CO_2 and contained 126 mM NaCl, 2.5 mM KCl, 26 mM $NaHCO_3$, 2 mM $CaCl_2$, 2 mM $MgCl_2$, 1.25 mM NaH_2PO_4, and 10 mM glucose. Hepes-buffered ACSF was saturated with 100% O_2, Hepes acid replaced $NaHCO_3$, and pH was titrated to 7.4 with NaOH. Recording pipettes were filled with 123 mM potassium gluconate, 2 mM $MgCl_2$, 8 mM NaCl, 10 mM Hepes, 1 mM EGTA, 4 mM potassium adenosine 5′-triphosphate, and 0.3 mM sodium guanosine 5′-triphosphate (pH 7.2). Similar results were obtained when pipettes were buffered with 16 mM $KHCO_3$ and 5% CO_2. Junction potentials were corrected and a saline-bridged ground was used. Selective synaptic $GABA_A$ receptor activation was produced by using the glutamate receptor blockers 6,7-dinitroquinoxaline-2,3-dione (DNQX, 20 μM) and kynurenic acid (1 mM) and the $GABA_B$ receptor blocker CGP-35348 (100 μM). Muscimol (250 μM) in Hepes ACSF was applied by pressure pulses (40 psi) of 5 to 100 ms through a 1-μm diameter pipette tip. Current-voltage data were fit with the constant field equation in the form $I = \text{perm}(A_{EC}VF^2/RT)\{1 - \exp[(V_0 - V)F/RT]/[1 - \exp(-VF/RT)]\}$, where I is the current, V is the membrane potential, $V_0 = E_{GABA}$, $A_{EC} = [Cl]_e + [HCO_3]_e$) ($\text{perm}_{HCO_3}/\text{perm}_{Cl}$) and perm is the ionic permeability (*30*).
22. As previously reported (*4, 5*), in HCO_3^--buffered ACSF, the waveform and reversal potential of the GABAergic depolarization varied as a function of the pipette placement and the amount of agonist ejected, because of variable activation of dendritic versus somatic $GABA_A$ receptors (compare Fig. 2F to Fig. 3B).
23. A. M. Tolkovsky and C. D. Richards, *Neuroscience* **22**, 1093 (1987); D. A. Nachson and P. Drapeau, *J. Gen. Physiol.* **91**, 289 (1988). Amiloride experiments were performed with direct agonist application to control for presynaptic effects due to inhibition of voltage-dependent Na^+ conductances [T. R. Kleyman and E. J. Cragoe, *Methods Enzymol.* **191**, 739 (1990)].
24. At very depolarized test potentials near E_{HCO_3}, the voltage-dependent ClC-3 Cl^- conductance was activated and Cl^- influx via ClC-3 caused E_{Cl} to shift toward the test potential before $GABA_A$ receptor activation. Thus, at these potentials, the $GABA_A$ current was carried primarily by a HCO_3^- flux, so that acetazolamide decreased the amplitude of the current, but the reversal potential was only shifted by −6 mV (n = 4) (*16*). When ClC-3 was blocked by 500 μM SITS (*30*), Cl^- influx before GABA receptor activation was blocked at depolarized test potentials, and E_{Cl} re-

mained negative to the test potential. Under these conditions, $GABA_A$ receptor activation produced a larger Cl^- flux, and acetazolamide induced a −18-mV shift in the reversal potential toward E_{Cl} (n = 4).
25. M. L. Mayer and G. L. Westbrook, *J. Physiol. (London)* **394**, 501 (1987).
26. L. Vyklicky Jr., V. Vlachova, J. Krusek, *ibid.* **430**, 497 (1990); S. F. Traynelis and S. G. Cull-Candy, *ibid.* **433**, 727 (1991).
27. $GABA_B$ antagonists enhance long-term potentiation (LTP) induction by high-frequency stimulation [C. H. Davies and G. L. Collingridge, *Pharmacol. Commun.* **2**, 98 (1992)], whereas $GABA_B$ agonists enhance LTP induction by lower frequency stimulation [D. D. Mott and D. V. Lewis, *Science* **252**, 1718 (1992); C. H. Davies, S. J. Starkey, M. F. Pozza, G. L. Collingridge, *Nature* **349**, 609 (1992)].
28. D. M. Woodbury and J. W. Kemp, in *Antiepileptic Drugs*, D. M. Woodbury and J. K. Penry, Eds. (Raven Press, New York, 1982), pp. 771–789.
29. M. A. Whittington, R. D. Traub, J. G. R. Jeffreys, *Nature* **373**, 612 (1995); H. B. Michelson and R. K. S. Wong, *J. Physiol. (London)* **477**, 35 (1994).
30. R. L. Smith, G. H. Clayton, C. L. Wilcox, K. W. Escuerdo, K. J. Staley, *J. Neuroscience*, **15**, 4057 (1995).
31. M. J. During *et al.*, *Nature* **376**, 174 (1995).
32. A. L. Hodgkin and B. Katz, *J. Physiol. (London)* **108**, 37 (1949).
33. The small, late outward component that is not affected by amiloride and acetazolamide is due to diffusion of muscimol toward somatic $GABA_A$ receptors, where the Cl^- gradient is more stable (*12, 19, 22*).
34. We thank T. Dunwiddie and R. Nicoll for helpful comments on the manuscript. Supported by NIH grants (NS01573, HD27827, and AA03527) and the American Epilepsy Foundation.

10 January 1995; accepted 30 May 1995

Recurrent Excitation in Neocortical Circuits

Rodney J. Douglas,* Christof Koch, Misha Mahowald, Kevan A. C. Martin, Humbert H. Suarez†

The majority of synapses in the mammalian cortex originate from cortical neurons. Indeed, the largest input to cortical cells comes from neighboring excitatory cells. However, most models of cortical development and processing do not reflect the anatomy and physiology of feedback excitation and are restricted to serial feedforward excitation. This report describes how populations of neurons in cat visual cortex can use excitatory feedback, characterized as an effective "network conductance," to amplify their feedforward input signals and demonstrates how neuronal discharge can be kept proportional to stimulus strength despite strong, recurrent connections that threaten to cause runaway excitation. These principles are incorporated into models of cortical direction and orientation selectivity that emphasize the basic design principles of cortical architectures.

The basic functional architecture of the neocortex, which forms 70 to 80% of the primate brain, is now well established: Neurons with similar functional properties are aggregated together, often in columns or swirling, slab-like arrangements. This architecture reflects the fact that, although lateral connections do occur between and across columns (*1*), most connections are made locally within the neighborhood of a 1-mm column, as Hubel and Wiesel (*2*) originally suggested (*3*).

The neocortex is dominated by excitatory connections. Eighty-five percent of synapses within the gray matter are excitatory and most of these synapses originate from cortical neurons (*4*). Moreover, about 85% of the 5000 to 10,000 synapses made by excitatory neurons are onto other excitatory neurons (*4, 5*), which suggests that excitatory corticocortical synapses must contribute strongly to the response characteristics of individual neurons. This view is in agreement with electrophysiological findings (*6*). In interpretations of cortical function, however, feedback excitation has been almost completely neglected in favor of a simple feedforward view (*2, 7*). But we now know, on the basis of anatomical evidence, that feedforward excitation from subcortical structures is not prominent: In the primary visual cortex of cats and primates, connections arising from the lateral geniculate nucleus (LGN) make up less than 10% of excitatory synapses formed with the input neurons of cortex layer IV spiny stellate cells (*8*). Most synapses onto spiny stellate cells originate from layer VI pyramids and other spiny stellate cells (*9*).

Given this massive excitation, which has been proposed to be a basic feature of cortical operation (*10*), can we infer the fraction of neurons that make first-order recurrent or reciprocal connections, in which two neurons directly excite each other (*11*)? We estimated the number of such recurrent connections for the spiny stellate cells of layer IV in the cat visual cortex from our detailed three-dimensional (3D) reconstructions of the axons and maps of the synapses they receive (*9*). The boutons of these cells usually occur in a few clusters (*12*). Approximation of the radial density of synaptic boutons in the cluster surrounding the soma by a 3D Gaussian distribution (characterized by its standard deviation σ; Fig. 1A) enables straightforward computation of the fraction of synapses onto a spiny stellate cell in layer IV (Fig. 1B). Even when we only consider synapses within this primary cluster, recurrent connections among spiny stellate cells can provide a significant source of recurrent excitation.

The electronic circuit analogy of Fig. 2A illustrates how recurrently connected neurons amplify current (*13*). The current-discharge curve of a single representative neuron shows that the discharge frequency is proportional to the excitatory current delivered to the soma. Discharge is represented by voltage in the electronic model; here, a conductance G (the value of which is inversely related to the slope of the current-discharge curve) will yield the discharge relation of a hypothetical linear neuron. The neuron's firing frequency F corresponds to the voltage across the conductance induced by the total current reaching the "soma" in our simple model of a neuron.

The simplest case of recurrent excitation occurs in a population of identical neurons, all receiving the same feedforward input current I_{ff} and forming identical synapses with each other. Any one neuron within this population contributes some excitatory current to each of its neighbors in the population and receives from all of them a recurrent feedback component I_{rec}. As a simple model of synaptic interaction, we assume that the current that flows into a neuron from an excitatory synapse is proportional to the discharge frequency of the presynaptic cell. Because all synapses and neurons are assumed to be identical, we can reduce this network to a single neuron that receives a recurrent current I_{rec} proportional to its own firing frequency F. This lumped recurrent synapse behaves as a voltage-controlled current source with an amplitude of αF, where α is the excitatory conductance. We can think of α as a phenomenological "network conductance" because it is generated by the activity of the network of neurons. At equilibrium, the firing rate of the network F^* must obey

$$I_{ff} + \alpha F^* = GF^* \quad (1)$$

(Fig. 2B). Thus, the output of the popula-

R. J. Douglas, Institute of Neuroinformatics, University and Eidgenössische Technische Hochschule, Zürich 8006, Switzerland; Computation and Neural Systems Program, 139-74, California Institute of Technology, Pasadena, CA 91125, USA; and Center for Biological and Medical Systems, Imperial College, London SW7 ZBT, UK.
C. Koch and H. H. Suarez, Computation and Neural Systems Program, 139-74, California Institute of Technology, Pasadena, CA 91125, USA.
M. Mahowald, Institute of Neuroinformatics, University and Eidgenössische Technische Hochschule, Zürich 8006, Switzerland, and Center for Biological and Medical Systems, Imperial College, London SW7 ZBT, UK.
K. A. C. Martin, Medical Research Council Anatomical Neuropharmacology Unit, Oxford OX1 3TH, UK.

*To whom correspondence should be addressed.
†Present address: Lancet Online Corporation, Kendall Square, Cambridge, MA 02139, USA.